pharmaceutics

MDPI

Article

Urea-Based Prodrugs Improve Systemic Mebendazole Exposure After Oral Administration

Katarina Färnegårdh [1], Richard Svensson [2], Prasad Wakchaure [1], Johanna Larsson [3], Christoffer Bengtsson [1], Claes Andersson [4], Rolf Larsson [4], Peter Nygren [5], Ylva Gravenfors [1,*,†] and Mårten Fryknäs [4,†]

[1] Science for Life Laboratory, Drug Discovery & Development Platform, Hit2Lead Medicinal Chemistry, Department of Biochemistry and Biophysics, Stockholm University, SE-171 21 Solna, Sweden; prasadwakchaure@gmail.com (P.W.); christoffer.bengtsson@scilifelab.se (C.B.)
[2] Science for Life Laboratory, Drug Discovery & Development Platform, Department of Pharmacy, Uppsala University, SE-751 23 Uppsala, Sweden; richard.svensson@uu.se
[3] Science for Life Laboratory, Drug Discovery & Development Platform, Department of Medicinal Chemistry, Uppsala University, SE-751 23 Uppsala, Sweden; johanna.larsson@scilifelab.uu.se
[4] Department of Medical Sciences, Division of Cancer Pharmacology and Computational Medicine, Uppsala University, SE-751 85 Uppsala, Sweden; claes.andersson@medsci.uu.se (C.A.); rolf.larsson@medsci.uu.se (R.L.); marten.fryknas@medsci.uu.se (M.F.)
[5] Department of Immunology, Genetics and Pathology, Uppsala University, SE-751 85 Uppsala, Sweden; peter.nygren@igp.uu.se
* Correspondence: ylva.gravenfors@dbb.su.se; Tel.: +46-706-724-897
† These authors contributed equally to this work.

Abstract

Background/Objectives: Mebendazole (MBZ) is an established anthelmintic drug with emerging therapeutic potential in oncology and immunology, but its broader clinical utility is constrained by poor aqueous solubility and extensive first-pass metabolism, resulting in low and variable systemic exposure. **Methods:** Here, we synthesized and profiled in vitro a series of solubility-enhanced, urea-based MBZ prodrugs designed to favor intact absorption across the intestinal epithelium followed by systemic release of parent MBZ. **Results:** Optimized candidates exhibited markedly improved solubility under simulated intestinal conditions and a favorable metabolic profile, including reduced intestinal metabolism compared with MBZ. In mouse pharmacokinetic studies, oral administration of selected prodrugs increased systemic MBZ exposure relative to equimolar doses of MBZ. Administration of the lead prodrug **2i** resulted in an approximately 10-fold higher peak MBZ concentration (C_{max}) and approximately 2-fold higher MBZ exposure (area under the plasma concentration–time curve, AUC) compared with an equimolar dose of MBZ. These differences should be interpreted in light of the different dosing formulations, with the prodrug administered as a solution and MBZ as a suspension. **Conclusions:** These findings provide in vivo proof-of-concept that urea-based prodrugs may improve systemic MBZ exposure following oral administration and support further evaluation of this strategy for indications requiring systemic drug exposure.

Keywords: mebendazole; urea-based prodrug; self-immolative linker; drug solubility enhancement; pharmacokinetic optimization; systemic exposure; drug repurposing; innovative drug design

Check for updates

Academic Editors: Federico Zappaterra and Pier Paolo Giovannini

Received: 27 September 2026
Revised: 29 October 2026
Accepted: 5 November 2026
Published: 9 November 2026

Copyright: © 2026 by the authors. Licensee MDPI, Basel, Switzerland. This article is an open access article distributed under the terms and conditions of the Creative Commons Attribution (CC BY) license.

1. Introduction

Mebendazole (MBZ) is an approved benzimidazole anthelmintic with extensive clinical experience in antiparasitic use [1,2]. This established clinical background makes MBZ

an attractive starting point for drug repurposing and further pharmaceutical development, since substantial information is already available regarding human use, tolerability, metabolism, and nonclinical safety [3–5]. Beyond its antiparasitic use, MBZ has attracted attention for potential applications in oncology [3,4,6], while immunological effects support potential utility in inflammatory [5] and autoimmune diseases such as systemic lupus erythematosus (SLE) [7]. At the same time, therapeutic applications outside intestinal parasitic infections require careful pharmacokinetic and safety considerations, particularly when the aim is to achieve higher and more sustained systemic exposure than typically obtained with conventional MBZ treatment.

A major challenge in translating the promising preclinical findings into clinical use in indications where systemic exposure is required is posed by the pharmacokinetic properties of MBZ, with both limited solubility and extensive first-pass metabolism contributing to its low and variable bioavailability. In a phase 2a study in patients with metastatic colorectal cancer, therapeutic systemic exposure could not be reliably achieved or maintained despite individualized high-dose oral MBZ treatment guided by therapeutic drug monitoring (TDM) [8]. Only a minority of the patients reached the predefined target concentration of 300 ng/mL, and in most cases this was achieved only transiently. Even at the maximum allowed daily dose, several patients remained below the target concentration range, and both inter- and intra-individual variability was high.

MBZ is classified as a class II drug in the Biopharmaceutics Classification System (BCS) [9]. Consequently, its absorption is considered limited by dissolution/solubility rather than permeability [1,2,10]. The very high melting point (>288.5 °C) reflects the high lattice energy and strong intermolecular interactions that must be overcome during dissolution. The relative oral bioavailability at therapeutic doses has been reported to be <5% due to the combination of very low solubility and high first-pass metabolism [1,2,10].

The mismatch between promising biological activity in preclinical models and poor clinical pharmacokinetic performance highlights the need for innovative approaches to enable the use of MBZ in indications requiring systemic exposure. Several strategies have been explored to address its low solubility, including polymorph selection [11–13], salt or cocrystal-based crystal engineering [14–16], solid dispersions [17,18], nanoemulsifying formulations [19], cyclodextrin complexation [20], and prodrug design [21–24]. Several groups have previously explored MBZ prodrugs as a strategy to address its low aqueous solubility and limited oral bioavailability (Figure 1a). The most comprehensive series of MBZ prodrugs to date was reported by Zimmermann et al. [24], who described the synthesis of N-substituted derivatives with improved aqueous solubility and oral bioavailability in preclinical in vivo models, as exemplified by their lead compound (**1d**) [24].

In the present work, we sought to build on these earlier findings while addressing a distinct pharmacokinetic question. Rather than designing prodrugs such as **1d,** which appears to undergo rapid pre-systemic bioactivation to MBZ, our aim was to identify soluble and permeable prodrugs that can be absorbed in intact form and then release MBZ post-absorption. We hypothesized that this strategy could increase systemic exposure of MBZ by addressing the low solubility and potentially also attenuating the extensive first-pass metabolism that has a substantial contribution from intestinal metabolism [10,25]. To this end, we designed urea-based MBZ prodrugs containing a masked internal N-nucleophile within a self-immolative linker (**2**) (Figure 1b). Following enzymatic unmasking, the internal nucleophile was hypothesized to promote intramolecular cyclization, rendering the urea labile and enabling the release of MBZ. To our knowledge, strategies in which a nitrogen atom in the parent drug is incorporated into a urea derivative and later activated as a leaving group have only rarely been described. One related example is tofacitinib using azo-reductase activation for colon-targeted delivery [26], which employs a different

delivery strategy compared to the prodrugs described herein, which were designed for intestinal absorption followed by systemic release of the parent molecule.

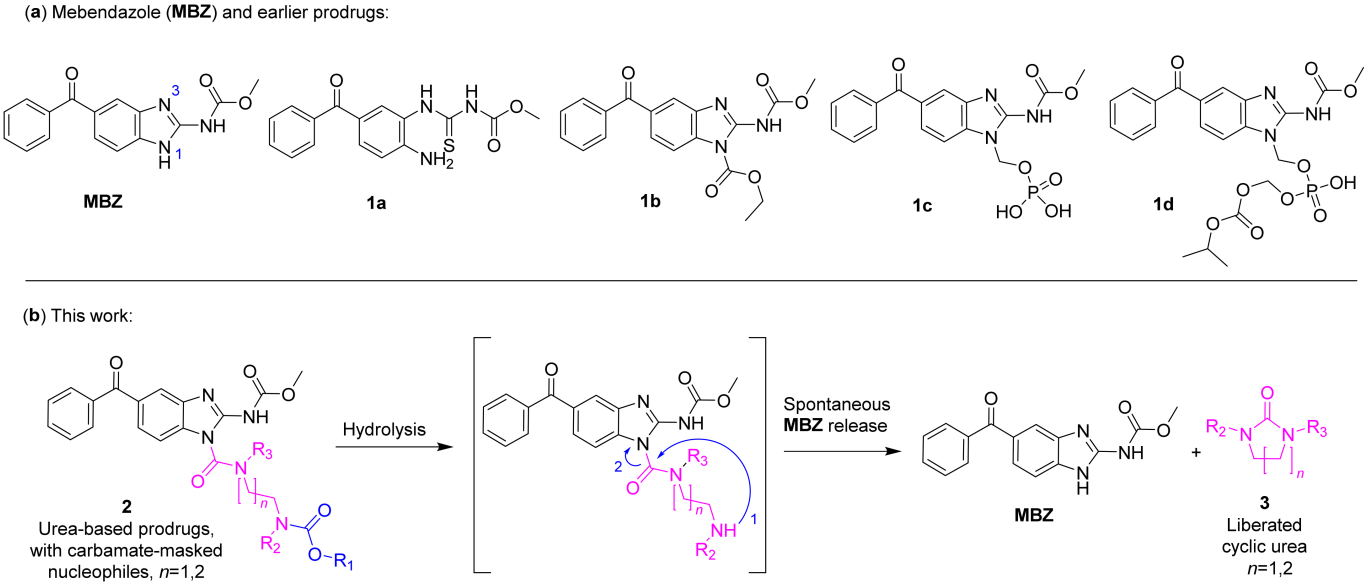


Figure 1. (**a**) Mebendazole (MBZ) and examples of previously described MBZ prodrugs. Dawson investigated a thiourea prodrug (**1a**) designed to produce MBZ through an enzymatically triggered cyclization reaction [21]. Other approaches have primarily relied on substitution of the endocyclic benzimidazole nitrogen to disrupt the crystal lattice of MBZ and/or introduction of solubilizing moieties. Examples include N-alkoxycarbonyl carbamate prodrugs (**1b**) described by Nielsen et al. [22] and a phosphonooxymethyl prodrug (**1c**) described by Chassaing et al. [23]. Prodrug **1d** is the lead compound in a series of N-substituted MBZ derivatives with improved aqueous solubility and oral bioavailability in preclinical in vivo models described by Zimmermann et al. [24]. (**b**) Schematic representation of urea-based prodrugs **2** described in this work, with a carbamate-masked (blue) nucleophile and a self-immolative linker (pink). MBZ and a cyclic urea **3** are hypothesized to be released following the triggering event in which the unmasked nucleophile is formed. The prodrugs utilizing a substituent on the endocyclic nitrogens are isolated as mixtures of regioisomers where the substituent is attached to the N^1 or N^3 position [22,24]. Only one representation is drawn here.

2. Materials and Methods

To identify prodrug candidates with a pharmacokinetic profile enabling improved systemic MBZ exposure, we established a screening cascade designed to reflect the expected in vivo sequence following oral administration (Figure 2). Taken together, this evaluation strategy was designed to test whether urea-based MBZ prodrugs could overcome the key pharmacokinetic limitations of MBZ and increase systemic parent drug exposure in vivo by remaining soluble and stable during gastrointestinal passage, being absorbed as intact prodrugs, and subsequently releasing MBZ.

2.1. Materials

MBZ-polymorph C sourced from Sigma Aldrich was used for benchmarking purposes. The two main metabolites of MBZ, 5-hydroxymebendazole (**6a**) (racemic) and mebendazole-amine (**6b**), were purchased from Sigma. The fragment **3i**, which is formed after the release of MBZ from the prodrug **2i**, was synthesized (see Supplementary Materials).

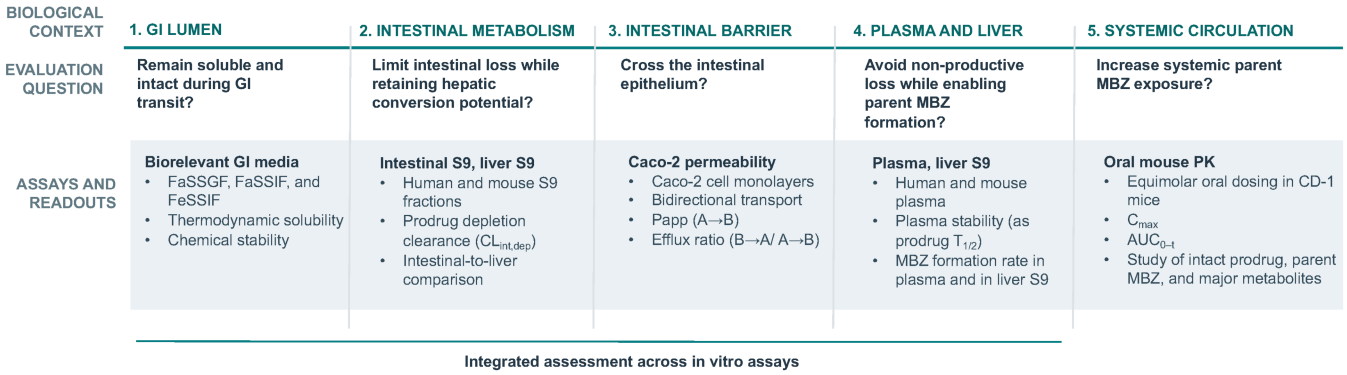


Figure 2. Assay-guided framework for evaluating urea-based MBZ prodrugs. The screening cascade organizes complementary assays according to the biological environments relevant to oral absorption and systemic exposure. The upper tier shows the biological context and the question addressed at each stage; the shaded tier lists the corresponding assays and readouts. The in vitro evaluation included thermodynamic solubility and chemical stability in biorelevant gastrointestinal media. Intestinal and hepatic subcellular fractions (S9) were used to distinguish prodrugs prone to intestinal pre-systemic metabolism from those with a profile more compatible with productive systemic formation of MBZ. The S9 experiments characterize metabolic potential in the respective preparations under the assay conditions but do not establish the major anatomical site of prodrug conversion in vivo. Caco-2 permeability as a means of understanding intestinal absorption was complemented by measurements of prodrug stability and MBZ formation in plasma together with bioactivation in liver S9 to determine whether metabolism could contribute to systemic parent drug exposure. Integrated profiles across these assays, rather than a single predefined numerical cutoff, were used to prioritize candidates for oral PK studies in mice where selected candidates were evaluated with regard to systemic exposure of MBZ, remaining prodrug, and major MBZ metabolites in vivo. MBZ, mebendazole; GI, gastrointestinal; FaSSGF, fasted-state simulated gastric fluid; FaSSIF, fasted-state simulated intestinal fluid; FeSSIF, fed-state simulated intestinal fluid; S9, supernatant fraction containing both cytosol and microsomes; P_{app}, apparent permeability; $CL_{int,dep}$, intrinsic clearance of prodrug depletion; A→B, apical-to-basolateral transport; B→A, basolateral-to-apical transport; $T_{1/2}$, half-life; PK, pharmacokinetics; C_{max}, maximum observed plasma concentration; $AUC_{0–t}$, area under the plasma concentration–time curve from time zero to the last quantifiable time point.

2.2. Synthesis of the Prodrugs

The starting materials and reagents used in preparing the prodrugs described herein are available from commercial suppliers or can be prepared using the methods published by others. Compound **1d** was synthesized according to Zimmermann et al. [24]. Synthetic descriptions and characterizations of the prodrugs are presented in the Supplementary Materials. Two regioisomers of the prodrugs were formed in reactions with MBZ due to the endocyclic benzimidazole nitrogen atoms being substituted either at the N^1 or N^3 position, as previously reported by others [22,24]. In addition, the NMR spectra of all the compounds containing the MBZ motif indicate the presence of rotamers. Therefore, for most of the prodrugs, the aromatic signals are reported as one signal and all aliphatic protons in the shift region 2.8–4.2 ppm are integrated together, showing the ratio between the aliphatic and the aromatic protons. The purity was more than 93% for all synthesized compounds, determined by HPLC (UV, for the prodrugs as mixtures of regioisomers) and the regioisomeric ratio was determined by HPLC (UV, peak1:peak2) based on the elution order of the peaks. Assignment of the peaks to the specific regioisomer was not performed.

2.3. Solubility and Chemical Stability in Simulated Gastric/Intestinal Fluids

Thermodynamic solubility was determined from solid material across three biorelevant media: fasted-state simulated gastric fluid at pH 1.6 (FaSSGF), fed-state simulated

intestinal fluid at pH 5.0 (FeSSIF), and fasted-state simulated intestinal fluid at pH 6.5 (FaSSIF). Biorelevant media were prepared using SIF Powder according to the manufacturer's instructions (Biorelevant.com, London, UK). Test compounds were weighed directly into conical vials, and biorelevant media were added (200 µL) to yield suspensions with target concentrations >2 mM. Vials were sealed and continuously agitated on a shaker (600 rpm) for 22–24 h at 37 °C to establish thermodynamic solid–solute equilibrium. Following incubation, the suspensions were transferred to glass inserts and centrifuged for 30 min at 10,000× *g* at 37 °C to cleanly separate undissolved solid material from the liquid phase. The saturated supernatant was collected, diluted (from 10- to 10,000-fold) in H_2O/acetonitrile (50:50 *v*/*v*), mixed 1:1 with acetonitrile containing warfarin as an internal standard, and analyzed by liquid chromatography–tandem mass spectrometry (LC-MS/MS). Analyte concentrations were quantified against a matrix-matched calibration curve.

Chemical stability was evaluated in solution to quantify intrinsic pH-dependent degradation kinetics in the same biorelevant fluids. Test compounds were spiked from DMSO stock solutions into pre-warmed biorelevant media to yield final concentrations of 4–10 µM, ensuring complete dissolution. Incubations were maintained at 37 °C under continuous agitation (600 rpm). Aliquots were withdrawn at 0, 1, and 24 h, quenched 1:1 with ice-cold acetonitrile containing warfarin as an internal standard, and stored at −20 °C or −80 °C prior to LC-MS/MS analysis in multiple reaction monitoring (MRM) mode. Chemical stability was expressed as the percentage of parent compound remaining relative to the 0 h baseline (set to 100%). Natural logarithm-transformed percentages were fitted to a linear regression model (assuming first-order elimination kinetics) to calculate the elimination rate constant (k), $T_{1/2} = \ln(2)/k$. For compounds exhibiting no detectable degradation over 24 h, the in vitro half-life ($T_{1/2}$) was reported as greater than the total incubation duration.

2.4. Caco-2 Permeability

A Caco-2 study to measure membrane permeability of test compounds was performed in accordance with published protocols [27]. Caco-2 cell monolayers (passage 94–105) were grown on Corning® HTS Transwell® 24-well Permeable Supports (Corning Incorporated, Corning, NY, USA)and used for the transport study on day 21 after seeding. Prior to the experiment, a test compound solution of 1–10 µM was prepared and warmed to 37 °C. The Caco-2 filters were washed with pre-warmed Hanks' Balanced Salt Solution (HBSS) prior to the experiment, and thereafter the experiment was started by applying the donor solution (containing the test compound) to the apical (A) or basolateral (B) side. The transport experiments were carried out at pH 7.4 in both the apical and basolateral chambers.

Enalaprilat was used as a membrane integrity control in each filter. The apparent permeability (P_{app}) of enalaprilat for a tight monolayer has been determined to be $<1 \times 10^{-6}$ cm/s. The experiments were performed at 37 °C with a stirring rate of 500 rpm. The receiver compartment was sampled at 30–60 min to calculate the mass balance of the test compound. The samples (100 µL) were transferred to a 96-well plate containing 100 µL methanol and warfarin as an internal standard and sealed until LC-MS/MS analysis. The samples were quantified using a separately constructed standard curve (from DMSO stock) in the same matrix as described above.

2.5. Hepatocyte Stability

Cryopreserved hepatocytes from CD-1 mice (Sekisui/Xenotech lot# 1810191, viability 67%; lot #1710229, viability 73%) were used in the experiments. The control experiments indicated good activity of the enzymes (midazolam and dextromethorphan/cytochrome P450 (CYP450) 3A4 and 2D6) within the cells. The cellular incubation concentration was 0.32–0.38 x 10^6 cells/mL. The incubation medium was Williams medium E with

4-(2-hydroxyethyl)-1-piperazineethanesulfonic acid (HEPES; 20 mM). The final test compound incubation concentration was 1 μM, prepared from 10 mM DMSO stocks. In brief, thawed and viability-checked cells at a 2× concentration were mixed with medium containing 2× test compound concentration to start the reaction. Aliquots (100 μL) were taken at 15, 30, 60 and 120 min and introduced into ice-cold acetonitrile containing warfarin as internal standard (100 μL) on a 96-well plate. The 0 min sample was constructed prior to the start of the reaction by taking aliquots (50 μL) from the 2 x solutions above. After the last time point, the plate was sealed, centrifuged (3500× *g*), and analyzed using LC-MS/MS. The analysis monitored the prodrug, MBZ, and major metabolites (**6a**, **6b**).

2.6. In Vitro S9 Incubation and Bioactivation Assays

Metabolic stability and parent drug bioactivation kinetics were determined using human intestinal S9 (HI-S9), human liver S9 (HL-S9), mouse intestinal S9 (MI-S9), and mouse liver S9 (ML-S9) fractions according to previously described protocols [25] with minor modifications. All S9 fractions were obtained from Xenotech LLC (BioIVT) and the product codes were H0610 for human and M1000 for mouse. S9 denotes the supernatant fraction containing both cytosol and microsomes.

Incubations were carried out in HPLC vials at 37 °C with continuous rotation at 600 rpm and were conducted at a nominal prodrug (substrate) concentration of 1 μM for the majority of compounds. For prodrugs **2b** and **2c**, HI-S9 and HL-S9 incubations were performed at 10 μM. Reaction mixtures contained test compounds (prodrug) or reference parent drug (MBZ) (final DMSO concentration 0.2% *v*/*v*) and 1 mM reduced nicotinamide adenine dinucleotide phosphate (NADPH) in 0.1 M potassium phosphate buffer (pH 7.4). Final total protein concentrations were maintained at 0.2 mg/mL for intestinal S9 fractions (HI-S9 and MI-S9) and 0.4 mg/mL for liver S9 fractions (HL-S9 and ML-S9).

Aliquots (100 μL) were collected at 5, 10, 20, 40, and 60 min or 0, 15, 30, and 60 min, and quenched immediately into 96-well plates containing 100 μL of ice-cold acetonitrile supplemented with warfarin as an internal standard. For "0-min" baseline controls, reaction components (NADPH stock, S9 stock, and compound buffer solution) were added individually into the quenching solvent. Plates were sealed, centrifuged (3500× *g*, 20 min, 4 °C), and the supernatants were analyzed by LC-MS/MS to simultaneously monitor prodrug depletion and parent drug (MBZ) formation.

The depletion rate constant (k_{dep}, min^{-1}) of each prodrug was calculated from the slope of the linear regression of the natural logarithm of the remaining analyte-to-internal standard peak area ratio versus incubation time. The intrinsic clearance of prodrug depletion ($CL_{int,\,dep}$, μL/min/mg protein) was calculated using Equation (1):

$$CL_{int,\,dep} = (k_{dep}/[\text{Protein}]) \times 1000 \quad (1)$$

where [Protein] is the S9 protein concentration in the incubation (mg/mL).

To avoid reporting artifactual degradation driven by analytical noise, an assay limit of quantification for prodrug depletion was defined based on a maximum detectable half-life equal to 5 times the total incubation duration ($t_{1/2,max} = 5 \times 60$ min $= 300$ min, corresponding to $k_{dep,\,min} = 0.00231\ min^{-1}$). Accounting for incubation protein levels ([Protein] = 0.2 mg/mL for intestinal S9; 0.4 mg/mL for liver S9), clearance values below or equal to the threshold criteria were designated as no detectable degradation:

$$\text{Intestinal S9 Limit: } CL_{int,\,dep} \leq 0.00231/0.2 \times 1000 = 12\ \mu L/min/mg$$

$$\text{Liver S9 Limit: } CL_{int,\,dep} \leq 0.00231/0.4 \times 1000 = 6\ \mu L/min/mg$$

The apparent rate of parent drug (MBZ) formation (v_{app}, pmol/min/mg protein) was derived from the initial linear slope of parent drug generation over time, normalized to incubation protein concentration using Equation (2):

$$v_{app} = \Delta[C_{MBZ}]/(\Delta t \times [Protein]) \quad (2)$$

where $\Delta[C_{MBZ}]/\Delta t$ represents the rate of MBZ formation (μM/min). Formed MBZ concentrations were estimated (semi-quantitative) via single-point calibration against the analyte-to-internal standard peak area ratio measured in t = 0 min samples of parent MBZ incubated concurrently under identical assay conditions at the same initial nominal concentration ($[S]_0$). For incubations conducted at 10 μM substrate concentration (**2b** and **2c**), calculated formation rates (v_{app}) were normalized by a factor of 10 to allow direct comparison with 1 μM incubation datasets, assuming pseudo-first-order bioactivation kinetics ($[S] \ll K_m$). K_m denotes the Michaelis constant.

2.7. Quantification by LC-MS/MS Analysis

All quantitative analyses were performed using LC-MS/MS. The mass spectrometry (MS) instrumentation used was either a Waters TQs micro or a SCIEX QTRAP 6500 in positive MRM mode coupled to a Waters Acquity ultra-performance liquid chromatography (UPLC) system. Reversed-phase chromatography was performed with mobile phases: A: 0.1% formic acid; B: acetonitrile and 0.1% formic acid. Separation was performed using an ACQUITY UPLC HSS T3 column (2.1 × 50 mm, 1.8 μm particle size; Waters Corporation, Milford, MA, USA) at 0.5 mL/min or an ACQUITY UPLC BEH C18 column (2.1 × 50 mm, 1.7 μm particle size; Waters Corporation, Milford, MA, USA) at 0.5 mL/min. The run time was 2–3 min. When monitoring the remaining prodrugs, the two regioisomers co-eluted on the column and the data given is the combined values in each case. Calibration curves were constructed over a dynamic range of 1–10,000 nM (or 10–10,000 nM, depending on matrix and assay) using 2nd-degree polynomial (quadratic) regression with 1/x weighting ($r^2 > 0.99$). The lower limit of quantification (LLOQ) was established as the lowest calibration standard (1 or 10 nM) exhibiting a signal-to-noise ratio S/N > 10 and accuracy within +/- 20%. This dynamic range was sufficient for the majority of bioanalytical samples; when analyte concentrations exceeded the upper limit of quantification, samples were appropriately diluted in the matching blank matrix prior to re-analysis.

2.8. Oral Mouse Pharmacokinetics of MBZ and Prodrugs **2b**, **2c** *and* **2i**

The in vivo pharmacokinetic studies were conducted by Adlego Biomedical AB and, for the later low-dose study, Legado Bioresearch, Sweden, acting as external contract research organizations. Study-specific animal characteristics, husbandry, sampling procedures, and deviations are provided in the Supplementary Materials.

The high-dose pharmacokinetic evaluation comprised two separate oral single-dose studies in CD-1 mice. In the first study, MBZ was compared with prodrugs **2b** and **2c**, whereas the second study compared MBZ with prodrug **2i.** Both studies were designed to characterize the plasma exposure of the administered compounds, the formation of parent MBZ from the prodrugs, and the major MBZ metabolites (**6a** and **6b**). For prodrugs **2b** and **2c**, the metabolite **6c** was also included in the pharmacokinetic (PK) analysis. Plasma levels of the different compounds were measured by LC-MS/MS analysis of plasma samples obtained from the CD-1 mice following administration of the test compounds.

The test compounds were administered at an equimolar dose to MBZ. Prodrugs **2b** (55.2 mg/kg), **2c** (47.5 mg/kg) and **2i** (50.0 mg/kg), or MBZ (30 mg/kg) were orally administered to CD-1 mice as a formulation containing the test compound and diluent comprising 99.5% ethanol (5% *v*/*v*), polysorbate 80 (5% *v*/*v*), polyethylene glycol 300

(PEG300; 20% *v*/*v*) and H_2O (70% *v*/*v*). The formulations were prepared as follows: 1) ethanol (EtOH) was added to polysorbate 80 and the mixture was then gently shaken to avoid foaming until a one-phase system with no visual signs of different phases was obtained; 2) the compounds were added to the preformed solutions and the mixtures were gently shaken; 3) PEG300 was added and the mixtures were gently shaken until thoroughly mixed; and 4) H_2O was added dropwise and the mixtures were vortexed. The prodrugs were dissolved in these formulations, while MBZ was a suspension. Nine mice were dosed for each dose group and 3 samples per animal. In the 2019 study, plasma sampling time points were 0, 0.25, 0.5, 1, 2, 4, 8, 12, and 32 h; in the 2021 study, they were 0.25, 0.5, 1, 2, 4, 8, 12, 24, and 32 h. Plasma samples were precipitated using 50 µL plasma and 150 µL methanol in the 2019 study, and 25 µL plasma and 175 µL methanol in the 2021 study, with warfarin as an internal standard. A standard curve was created in blank CD-1 mouse plasma. The samples were centrifuged and analyzed as described below.

All quantitative analyses were performed using LC-MS/MS and against a standard curve constructed in the same matrix. The instrumentation used was a Sciex QTRAP 6500 coupled to a Waters Acquity UPLC. Mobile phases A: 0.1% formic acid; B: 95% methanol; 0.1% formic acid. Separation was performed on an HSS T3 C18 2 × 50 mm column at 0.5 mL/min. Run time 2.5 min. Gradient: 0 min/10% B–0.5 min/10% B; 0.5 min/10% B–1.5 min/60% B; 1.5 min/60% B–1.8 min/95% B; 1.8 min/95% B–2.2 min/95% B; 2.2 min/95% B–2.4 min/10% B; 2.4 min/10% B–2.5 min/10% B. For the sparse-sampling pharmacokinetic studies, AUC_0–t was calculated from the mean plasma concentration–time profiles using the linear trapezoidal rule in GraphPad Prism (Version 10). Here, t represents the last quantifiable time point included in the respective concentration–time profile. As individual animals were not sampled at every time point, individual-animal AUC values could not be determined. The standard errors (SEs) associated with the composite AUC estimates were obtained from the GraphPad Prism analysis and were not interpreted as standard deviations of individual-animal AUC values. Other pharmacokinetic calculations and plots were generated using GraphPad Prism or a Microsoft Excel-based noncompartmental PK calculation tool.

In addition, prodrug **2i** was administered at a lower dose (16.8 mg/kg) and compared to the equimolar dose of MBZ (10 mg/kg) (see supporting information).

2.9. In Vitro Cytotoxicity Assessment

The cytotoxicity of MBZ, MBZ metabolites (**6a, 6b**), prodrug **2i**, and the fragment (**3i**) was assessed using the fluorometric microculture cytotoxicity assay (FMCA), which is based on the measurement of fluorescence generated using hydrolysis of fluorescein diacetate (FDA) to fluorescein by cells with intact plasma membranes.

The HepG2 cell line (American Type Culture Collection, ATCC; HB-8065) was cultured in Eagle's Minimum Essential Medium (ATCC) supplemented with 10% fetal bovine serum, Penicillin/Streptomycin (100 U/100 µg/mL) and L-glutamine 2 mM (all from Sigma St Louis, MO, USA). HepG2 cells were passaged 2 times/week and used for a maximum of 20 passages. Cells were finally seeded in Nunc 384-well assay plates (Nunc A/S, Thermo Fisher Scientific, Roskilde, Denmark) at a density of 1000 cells/well.

HepG2 cells (1000/well) were seeded in 384-well plates using the pipetting robot Biomek 4000 (Beckman Coulter, Fullerton CA, USA) and cultured overnight before drugs were added by acoustic dispensing (Echo 550 from Labcyte Inc, CA, USA) directly from 384-well source plates (Labcyte) containing 5–10 mM compound stock solutions in DMSO. Each drug was dispensed in dose–response, with eight two-fold dilutions in duplicate from top concentrations to generate half-maximal inhibitory concentration (IC_{50}) values.

Bortezomib (2 µM) was used as a positive control and dose–response testing of doxorubicin (top concentration 2 µM) was performed repeatedly to follow assay performance over time.

After 72 h of incubation with drugs in a culture chamber (at 37 °C, humidity 95%, 5% CO_2), the 384-well plates were centrifuged (200 g, 60 s), the culture medium was removed using a Biotek ELX washer (Biotek, Winooski, VT, USA), and 70 µL phosphate-buffered saline (PBS, Sigma) was added to the wells. This procedure was repeated once. Subsequently, the plates were centrifuged (200 g, 30 s) and the PBS was removed by the ELX washer, after which 50 µL/well of assay buffer (HEPES-buffered saline with 0.5 mM $MgCl_2$ and 0.5 mM $CaCl_2$, pH 7.4) was added to the plates using a EL406 (Agilent Technologies Inc., Santa Clara, CA, USA) and finally 1 µL of fluorescein diacetate (0.5 mg/mL in DMSO) was added to each well using the pipetting robot Biomek NX (Beckman Coulter, Fullerton CA, USA). The plates were then incubated for 50 min in a Cytomat (37 °C, humidity 95%, 5% CO_2, Thermo Fischer Scientific) before being analyzed in a Fluostar Omega (BMG LABTECH, Ortenberg, Germany) with wavelengths set at ex 485/em 530 nm.

Cytotoxicity was assessed after 72 h with cell survival presented as a survival index (SI, %) defined as fluorescence in test wells as a percentage of that in control cultures with blank values subtracted. Criteria for a successful assay included a signal-to-noise ratio in control cultures >10, coefficient of variation (CV) < 30% and a positive control (Bortezomib) SI of <5%. The half-maximal inhibitory concentration (IC_{50}) was determined from log concentration-effect curves in Graph Pad Prism (GraphPad software Inc., CA, USA) using non-linear regression analysis.

3. Results and Discussion

3.1. Design and Synthesis of Prodrug Candidates

In our first prodrug attempts, following the strategy of Nielsen et al. [22], we observed that derivatizing MBZ by the formation of carbamates at the endocyclic nitrogen atom yielded prodrugs with low chemical stability, resulting in the hydrolysis of even the solid material. Instead, we turned our attention to exploring a urea-based scaffold. The urea derivatives of MBZ were synthesized via a one-pot acylation reaction between deprotonated MBZ and the corresponding electrophile in N,N-dimethylformamide (DMF). The MBZ molecule exists as prototopic tautomers, and thus any of the benzimidazole nitrogen atoms may be substituted, leading to mixtures of products. Under the experimental conditions used here, the products were isolated as mixtures of N^1- and N^3-derivatized regioisomers, similar to those described previously [22,24].

The first urea investigated (**4**, Figure 3a) showed increased solubility, indicating a potential to break the strong stacking interactions in the crystal lattice and thereby address the brick-dust properties by urea formation on the benzimidazole nitrogen. Compound **4** showed 5-fold improved solubility compared to MBZ in biofluids simulating the small intestinal environment under fed and fasted conditions, FeSSIF (pH 5.0, solubility 200 µM) and FaSSIF (pH 6.5, solubility 240 µM), respectively, whereas the solubility in FaSSGF, simulating stomach pH in the fasted state (pH 1.6, solubility 200 µM), was similar to that of MBZ. However, to our disappointment, no formation of MBZ was detected when compound **4** was incubated with hepatocytes.

With these results in hand, we hypothesized that the introduction of an internal nucleophile potentially could assist the formation of MBZ, still taking advantage of both the increased solubility and high chemical stability of compound **4**. We wanted to investigate whether the stability of the urea-based prodrug could be tuned by the introduction of a distant nucleophile as part of a self-immolative linker that could release MBZ in an intramolecular cyclization reaction triggered by events unmasking the nucleophile. The nucleophile would initially need to be masked, preferably by a substituent that can be

removed, for example, by hydrolysis once the prodrug has entered the systemic circulation. For a schematic representation of the hypothesized release mechanism, see Figure 1b.

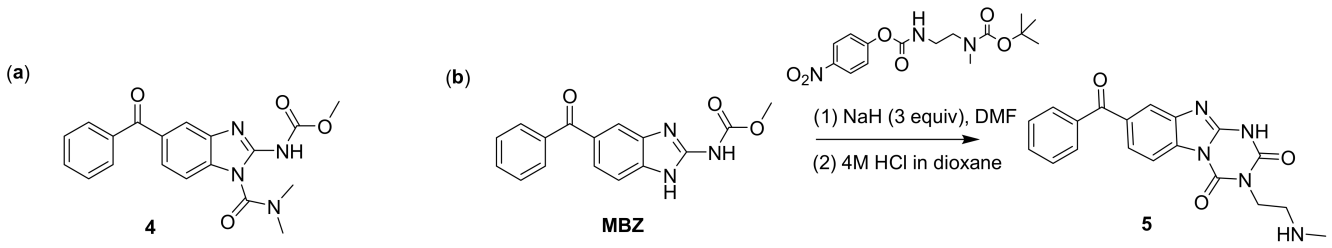


Figure 3. (**a**) First synthesized urea, **4** (one of the formed regioisomers drawn). (**b**) Synthetic route for the second attempt of preparing a urea-based prodrug containing a linker motif furnished cyclized compound **5**, revealing the need for a tertiary urea. DMF, N,N-dimethylformamide; MBZ, mebendazole.

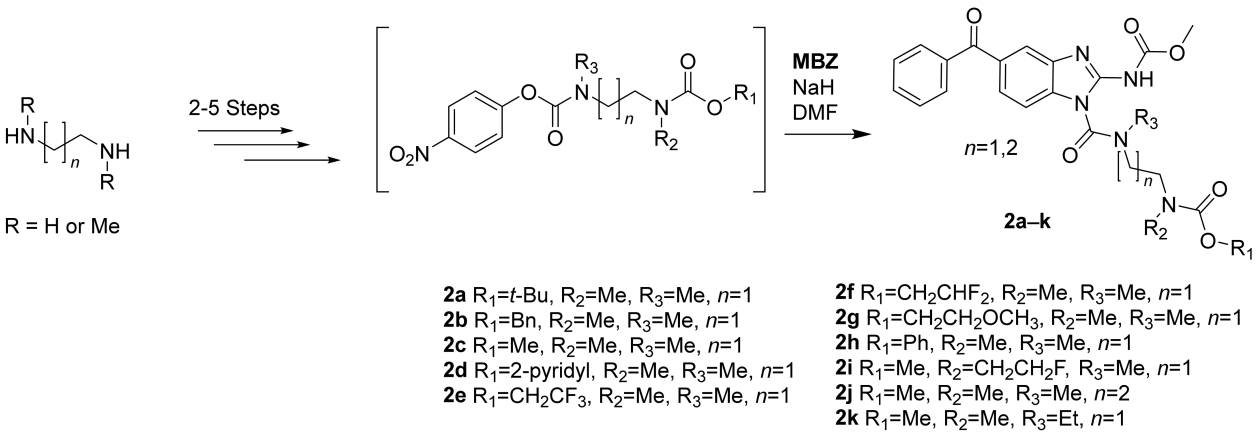
To test our hypothesis, MBZ was reacted with tert-butyl methyl(2-(((4-nitrophenoxy)carbonyl)amino)ethyl)carbamate under alkaline conditions using an excess of NaH (Figure 3b) (see Supplementary Materials). The isolated product was treated with 4 M HCl in dioxane for an acid-assisted hydrolysis of the carbamate masking the internal nucleophile to initiate the hypothesized cascade leading to the formation of MBZ. However, not even traces of MBZ were detected, but instead a new compound had formed, which after NMR investigation (see Supplementary Materials) was identified as the cyclized compound **5.** Thus, these initial attempts with urea-based prodrugs showed a need for an additional substituent on the urea to prevent an intramolecular attack on the MBZ carbamate under these strongly basic reaction conditions.

Our third attempt at investigating the urea-based approach included the synthesis of prodrugs **2a** and **2b** (Scheme 1; Table 1). In an experiment designed to evaluate our approach, where **2a** was treated with acid to unmask the internal nucleophile, the desired formation of MBZ was seen, supporting our hypothesis that urea motifs can be introduced as part of a prodrug strategy. To understand whether the prodrugs could also release MBZ at neutral pH, better reflecting more physiological conditions, debenzylation of **2b** was performed using hydrogenation with palladium on carbon in methanol (MeOH). Gratifyingly, the debenzylation showed around 50% conversion to MBZ after 1 h, with no trace of remaining non-cyclized unmasked N-nucleophile, indicating fast and spontaneous formation of MBZ under neutral conditions once the masking benzylic carbamate had been removed.

Encouraged by mechanistic studies, we next investigated whether MBZ could be formed from prodrug **2b** in mouse hepatocytes. We wanted to test our hypothesized concept where hepatic metabolic activation would unmask the internal nucleophile and thereby trigger the intramolecular cyclization reaction that makes MBZ a leaving group. It was clear that whereas prodrug **4** did not efficiently produce MBZ, prodrug **2b** generated MBZ at a rate of 26 pmol/min/1E6 cells. This was an important step to validate our hypothesis and to lay the groundwork for further investigation of our novel prodrugs in proof-of-concept experiments in vivo.

Building on these results, we were encouraged to further explore the potential of this structural class of MBZ prodrugs. Nine additional urea-based prodrugs (**2c**–**2k**) were designed and synthesized to improve our understanding of how the release rate of MBZ would be influenced by steric and/or electronic properties of substituents in different positions. Since the desired release mechanism is triggered by initial hydrolysis of the masking carbamate, which can occur either chemically or through the action of metabolizing enzymes such as esterases [28], six different R1 substituents were included in the design

to give a set of prodrugs addressing both steric and electronic properties of the masking carbamate to study its impact on the initial triggering step.



2a R_1=*t*-Bu, R_2=Me, R_3=Me, *n*=1
2b R_1=Bn, R_2=Me, R_3=Me, *n*=1
2c R_1=Me, R_2=Me, R_3=Me, *n*=1
2d R_1=2-pyridyl, R_2=Me, R_3=Me, *n*=1
2e R_1=CH_2CF_3, R_2=Me, R_3=Me, *n*=1
2f R_1=CH_2CHF_2, R_2=Me, R_3=Me, *n*=1
2g R_1=$CH_2CH_2OCH_3$, R_2=Me, R_3=Me, *n*=1
2h R_1=Ph, R_2=Me, R_3=Me, *n*=1
2i R_1=Me, R_2=CH_2CH_2F, R_3=Me, *n*=1
2j R_1=Me, R_2=Me, R_3=Me, *n*=2
2k R_1=Me, R_2=Me, R_3=Et, *n*=1

Scheme 1. Commercially available alkyl diamines (optionally protected) were converted to para nitrophenyl-activated carbamates suitable for base-mediated reaction with mebendazole (MBZ). Prodrugs (**2a**–**2k**) were formed as two regioisomeric products following substitution on either the N^1 or the N^3 of MBZ. For simplicity, only one structure is drawn here. The experimental description of the separate steps is summarized in the Supplementary Materials. Bn, benzyl; DMF, N,N-dimethylformamide; Et, ethyl; Me, methyl; Ph, phenyl; *t*-Bu, *tert*-butyl.

Table 1. Substitution pattern and linker length for each of the synthesized prodrugs **2a**-**2k**.

Compound	R_1 *	R_2 *	R_3 *	*n* *
2a	*t*-Bu	Me	Me	1
2b	Bn	Me	Me	1
2c	Me	Me	Me	1
2d	2-pyridyl	Me	Me	1
2e	CH_2CF_3	Me	Me	1
2f	CH_2CHF_2	Me	Me	1
2g	$CH_2CH_2OCH_3$	Me	Me	1
2h	Ph	Me	Me	1
2i	Me	CH_2CH_2F	Me	1
2j	Me	Me	Me	2
2k	Me	Me	Et	1

* R_1, R_2, R_3 and *n* refer to the structures in Scheme 1. Bn, benzyl; Et, ethyl; Me, methyl; Ph, phenyl; *t*-Bu, *tert*-butyl.

In addition to addressing the triggering step, i.e., hydrolysis of the masking carbamate, other factors that could influence the kinetics of the cyclization step such as linker length, nucleophilicity of the nitrogen (by varying R2) and steric properties (R3 variation) were also considered in the design. Saari et al. [29] demonstrated that structural modifications of the linker in a carbamate prodrug motif can have a pronounced effect on the kinetics of the intramolecular cyclization and subsequent drug release. Since the overarching goal of the prodrug strategy was to effectively produce MBZ, we anticipated that it was likely in our favor to have small and electron-donating R2 substituents (e.g., Me), although, at this stage, we did not know what the optimal kinetics would be. Upon completion of

synthesis, purification, and characterization (see Supplementary Materials), the prodrugs were evaluated according to the screening cascade (Figure 2).

3.2. In Vitro Characterization

3.2.1. Solubility and Chemical Stability

Given the aim of improving systemic MBZ exposure after oral administration, gastrointestinal solubility and stability were considered to be key prodrug properties. Solubility was therefore evaluated in biorelevant media reflecting fasted and fed gastrointestinal conditions, as differences in pH and fluid composition may affect prodrug solubility [30–33]. Stability was assessed in the same media, since prodrugs intended for oral absorption should remain sufficiently intact during gastric and intestinal passage.

The initial mechanistic compounds **4**, **2a**, and **2b**, together with the expanded prodrug series **2c**–**2k**, were evaluated in these assays. MBZ polymorph C, present in the commercial product Vermox™, was chosen as a reference compound, since different MBZ polymorphs have been reported to vary in solubility, therapeutic efficacy, and toxicity [11–13,34,35]. The previously described prodrug **1d** was also included as a benchmark for comparison with an earlier MBZ prodrug strategy [24].

Most of the urea-based prodrugs displayed markedly enhanced solubility relative to MBZ in simulated intestinal fluids, alongside excellent stability in media representing both fasted and fed conditions (Table 2; Table S1). An exception was prodrug **2a**, which was deprioritized due to reduced stability under acidic conditions. Its half-life ($T_{1/2}$) of 16 h in simulated fasted gastric fluid suggests increased susceptibility to premature gastric hydrolysis, which could compromise intact absorption across the intestinal epithelium. Encouragingly, the broader series of our urea-based prodrugs combined enhanced intestinal solubility with robust chemical stability.

Table 2. Solubility in intestinal fluids representing three different gastrointestinal (GI) conditions. FaSSGF, fasted-state simulated gastric fluid; FaSSIF, fasted-state simulated intestinal fluid; FeSSIF, fed-state simulated intestinal fluid; MBZ, mebendazole.

Compound	Solubility (µM) FaSSGF; pH 1.60	Solubility (µM) FeSSIF; pH: 5.00	Solubility (µM) FaSSIF; pH 6.50
MBZ	190	40	50
1d	6700	9800	6700
4	200	200	240
2a	Not determined	520	230
2b	17	330	76
2c	510	1200	980
2d	140	480	580
2e	100	210	190
2f	70	350	450
2g	3640	>2400	3450
2h	120	130	170
2i	960	990	1050
2j	280	820	750
2k	30	830	420

3.2.2. Compartmental Metabolism and Bioactivation in S9 In Vitro Systems

Having identified prodrugs with acceptable aqueous solubility and chemical stability, we next evaluated whether their metabolic turnover and bioactivation kinetics aligned with our targeted prodrug hypothesis, i.e., decreased intestinal metabolism relative to MBZ paired with efficient hepatic cleavage to release the parent MBZ into systemic circulation. To evaluate compartmental bioactivation, intestinal and hepatic S9 fractions were selected as the primary in vitro model. The S9 fraction contains both microsomal and cytosolic enzymes (including carbonyl reductases, carboxylesterases, CYP450 enzymes, etc.), representing clearance and bioactivation of the mucosal metabolic barrier and liver. Both human and mouse S9 fractions were evaluated to assess cross-species consistency to support the planned in vivo mouse pharmacokinetic studies. Assays monitored both overall prodrug depletion ($CL_{int,\ dep}$) and the apparent formation rate of the parent MBZ (v_{app}) (Table 3A,B and Figure S2). Rather than providing direct quantitative extrapolations to in vivo clearance (as no scaling factors were applied), these values allowed relative classifications of prodrugs within each system. A clearance threshold of $CL_{int,\ dep} \leq 12$ µL/min/mg was set as the quantification limit for prodrug depletion in intestinal S-9, and $CL_{int,\ dep} \leq 6$ µL/min/mg for liver S-9.

Consistent with previous reports [25], parent MBZ displayed higher intrinsic clearance in intestinal S9 fractions than in liver S9 fractions in both species ($CL_{int,\ dep}$ = 60 vs. 26 µL/min/mg in human; 26 vs. 17 µL/min/mg in mouse). Our primary objective was to identify prodrugs with increased intestinal stability relative to MBZ to enable intact intestinal mucosal permeation prior to hepatic bioactivation. Several prodrugs exhibited a similar or lower human intestinal-to-hepatic clearance ratio than MBZ (Table 3A, Depletion ratio HI-S9/HL-S9), indicating improvements in human intestinal stability compared to MBZ. In HI-S9, prodrugs **2g** and **2k** demonstrated negligible degradation, while compounds **2c**–**2f**, **2h**, and **2i** exhibited moderate clearance rates (19–56 µL/min/mg).

To follow productive prodrug metabolism once the prodrugs reach the systemic circulation, parent MBZ generation was quantified (v_{app}). In the human fractions, all evaluated prodrugs demonstrated different degrees of hepatic S9 bioactivation, supporting our prodrug strategy that MBZ may be formed from the prodrugs once they have passed the intestinal border. Prodrug **2j** was deprioritized from further studies due to excessive intestinal degradation, whereas **2b**, which exhibited the highest intrinsic clearance together with a fast rate of MBZ formation in this static in vitro system, was retained to analyze how distinct in vitro degradation profiles translate into in vivo exposure to MBZ.

In mouse S9 incubations, intestinal turnover was generally lower than in humans, with the majority of prodrugs exhibiting $CL_{int,\ dep} \leq 12$ µL/min/mg (Table 3B). Absolute rates of MBZ formation were elevated in mouse S9 fractions relative to human S9 fractions ($v_{app,\ ML\text{-}S9}$ = 14–90 pmol/min/mg), also supporting bioactivation in mouse hepatic S9. Cross-species comparison of the intestinal-to-hepatic clearance ratio showed a similar pattern for prodrugs **2b**, **2g**, **2h**, **2i**, and **2k**.

Importantly, these tissue-derived S9 assays demonstrate the overall enzymatic capacity to execute the initial carbamate unmasking step, but they do not identify the contributions of individual enzymes or enzyme isoforms (e.g., relative contributions of carboxylesterase 1 (CES1) vs. carboxylesterase 2 (CES2)). In early discovery screening, these subcellular incubations serve as comparative in vitro metrics rather than direct quantitative predictors of absolute in vivo clearance or bioactivation kinetics. Overall, these results provide a supportive rationale for selecting lead candidates for subsequent in vivo pharmacokinetic evaluation.

Table 3. (**A**) Metabolic depletion of MBZ and prodrugs, parent MBZ formation, and tissue selectivity in human S9 fractions. (**B**) Metabolic depletion of MBZ and prodrugs, parent MBZ formation, and tissue selectivity in mouse S9 fractions.

(**A**)

Compound	HI-S9 $CL_{int,\ dep}$ (μL/min/mg)	HL-S9 $CL_{int,\ dep}$ (μL/min/mg)	HI/HL Depletion Ratio	HI-S9 Apparent MBZ Formation, v_{app} ** (pmol/min/mg)	HL-S9 Apparent MBZ Formation, v_{app} ** (pmol/min/mg)
MBZ	60	26	2.3		
2b †	160	200	0.8	4.4	14.9
2c †	56	21	2.7	0.5	1.8
2d	44	13	3.4	1.8	10.0
2e	52	21	2.5	4.2	12.0
2f	30	16	1.9	6.7	17.0
2g	≤12 *	20	≤0.6	1.3	2.1
2h	48	51	0.9	1.1	6.8
2i	19	43	0.4	2.1	6.6
2j	150	49	3.1	3.9	13.0
2k	≤12 *	39	≤0.3	1.9	8.5

(**B**)

Compound	MI-S9 $CL_{int,\ dep}$ (μL/min/mg)	ML-S9 $CL_{int,\ dep}$ (μL/min/mg)	MI/ML Depletion Ratio	MI-S9 Apparent MBZ Formation, v_{app} ** (pmol/min/mg)	ML-S9 Apparent MBZ Formation, v_{app} ** (pmol/min/mg)
MBZ	26	17	1.5		
2b †	82	270	0.3	78	90
2c †	≤12 *	36	≤0.3	9	26
2d	≤12 *	13	≤0.9	12	25
2e	≤12 *	38	≤0.3	17	32
2f	13	30	0.4	30	49
2g	≤12 *	15	≤0.8	11	14
2h	≤12 *	38	≤0.3	24	34
2i	≤12 *	18	≤0.7	19	42
2j	≤12 *	19	≤0.6	24	38
2k	≤12 *	44	≤0.3	34	51

† Incubated at an initial prodrug concentration ($[S]_0$) of 10 μM (all other compounds incubated at 1 μM). The v_{app} values for **2b** and **2c** are normalized to 1 μM prodrug equivalents. Measured $CL_{int,\ dep}$ values at 10 μM represent conservative lower-bound estimates if enzyme saturation occurs ($[S] \approx K_m$). * Below the lower limit of quantification for prodrug depletion; see Section 2. ** Apparent rate of parent MBZ formation (v_{app}), estimated via single-point calibration. $CL_{int,dep}$, intrinsic clearance of prodrug depletion; HI, human intestinal; HL, human liver; HI-S9, human intestinal S9; HL-S9, human liver S9; MBZ, mebendazole; S9, supernatant fraction containing both cytosol and microsomes; v_{app}, apparent rate of parent MBZ formation; MI, mouse intestinal; ML, mouse liver; MI-S9, mouse intestinal S9; ML-S9, mouse liver S9.

3.2.3. Intestinal Permeability and Efflux Evaluation (Caco-2)

While oral bio-delivery and systemic exposure are collectively governed by aqueous solubility, membrane permeability, and pre-systemic first-pass metabolism [27,36–39], evaluating mucosal transport is essential to confirm that intact prodrug can cross the intestinal epithelium. We therefore evaluated intestinal permeability using Caco-2 cell monolayers, assessing both the apparent permeability coefficient ($P_{app,\ A\to B}$) and efflux ratio ($ER = P_{app,\ B\to A}/P_{app,\ A\to B}$) to characterize absorptive transport and active efflux liabilities

(Table 4). Standard classification criteria designate $P_{app, A\rightarrow B}$ >10 × 10^{-6} cm/s as high permeability and $P_{app, A\rightarrow B}$ < 1 × 10^{-6} cm/s as low permeability [27,39]. A threshold of $P_{app, A\rightarrow B}$ >5 × 10^{-6} cm/s was applied herein to select candidates for subsequent studies according to the screening cascade.

Table 4. Permeability in the Caco-2 cell assay.

Compound	Caco-2 P_{app} A→B (10^{-6} cm/s)	Caco-2 Efflux Ratio B→A/A→B (ER)
MBZ	230	0.7
1d	0.19	Not relevant *
4	140	0.9
2a	13	12
2b	12	16
2c	17	11
2d	2.1	91
2f	9.1	21
2g	9.2	14
2h	66	1.9
2i	43	3.6
2k	65	2

* The prodrug is hydrolyzed at the brush border and shows very low intrinsic permeability as the intact prodrug. A→B, apical-to-basolateral transport; B→A, basolateral-to-apical transport; ER, efflux ratio; MBZ, mebendazole; P_{app}, apparent permeability.

Unmodified MBZ exhibited high absorptive flux ($P_{app, A\rightarrow B}$ = 230 × 10^{-6} cm/s; ER = 0.7), confirming its BCS Class II status, where oral absorption is limited by the dissolution rate rather than membrane permeation [40]. Conversely, benchmark phosphate prodrug **1d** showed minimal intact transport ($P_{app, A\rightarrow B}$ = 0.19 × 10^{-6} cm/s), illustrating the severe permeability penalty often associated with highly ionized solubilizing handles.

Notably, despite displaying elevated efflux ratios (ER = 12 resp 16), our early urea-based prodrugs (**2a** and **2b**) maintained strong absorptive permeability ($P_{app, A\rightarrow B}$ = 13 resp 12 ×10^{-6} cm/s), exceeding our screening threshold. These results demonstrate appreciable apparent absorptive permeability, despite elevated efflux ratios under the experimental conditions. However, the extent to which efflux transport limits intestinal absorption in vivo remains uncertain, as transporter saturation and luminal drug concentrations were not directly investigated [41,42]. Except for **2d**, where increasing the polarity by the introduction of an extra H-bond acceptor penalized permeability and increased efflux ($P_{app, A\rightarrow B}$ = 2.1 × 10^{-6} cm/s; ER = 91), the entire urea-based series successfully combined enhanced aqueous solubility with mucosal permeability at a level considered sufficient for efficient intact absorption prior to systemic bioactivation

3.2.4. In Vitro Assessment of Systemic Plasma Stability and Parent MBZ Bioactivation

To determine whether intact prodrugs surviving intestinal transport can undergo systemic bioactivation to release parent MBZ, stability and biotransformation rates were evaluated in human and mouse plasma (Table 5)

Table 5. Stability and rate of parent MBZ bioactivation in human and mouse plasma.

Compound	Human $T_{1/2}$ (h)	Human MBZ Formation Rate * (h^{-1})	Mouse $T_{1/2}$ (h)	Mouse MBZ Formation Rate * (h^{-1})
2b	>14	0.37	>2.6	1.05
2c	>14	0.73	>2.6	1.25
2e	>14	1.37	>2.6	1.62
2f	>14	1.13	>2.6	2.1
2g	>14	0.56	>2.6	1.54
2h	>14	0.62	>2.6	0.65
2i	>14	0.36	>2.6	1.78
2k	>14	0.28	1.3 **	0.05

* Estimated from the appearance rate of parent MBZ over time (linear slope, h^{-1}). ** Undergoes apparent undesired degradation in mouse plasma yielding unproductive metabolites. MBZ, mebendazole; $T_{1/2}$, half-life.

In human plasma, all evaluated prodrugs demonstrated high stability ($T_{1/2} > 14$ h) with low-to-moderate rates of parent MBZ release (0.28–1.37 h^{-1}). This confirms that acellular plasma-mediated hydrolysis alone is slow, indicating that systemic bioactivation in humans will be primarily driven by liver metabolism (as demonstrated in hepatic S9 incubations) or potential cellular blood components (e.g., erythrocyte esterases).

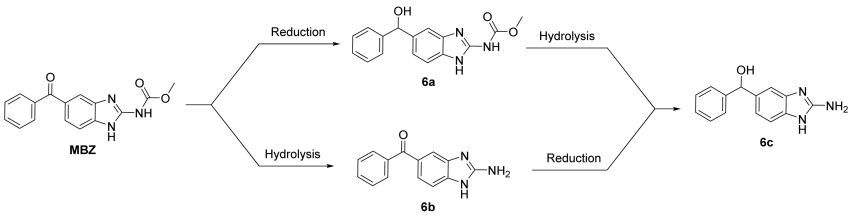
In mouse plasma, the stability was generally lower ($T_{1/2} > 2.6$ h for most candidates) alongside higher rates of MBZ formation (0.65–2.1 h^{-1}), consistent with the well-known presence of active circulating carboxylesterases in rodents. However, prodrug **2k** exhibited an undesired plasma profile with a short half-life in mouse plasma ($T_{1/2} = 1.3$ h) paired with negligible parent MBZ formation (0.05 h^{-1}). This rapid degradation into unproductive metabolites in systemic circulation deprioritized **2k** at this stage, when the next step would be in vivo PK studies in mice.

3.3. In Vivo Pharmacokinetics

The in vivo pharmacokinetic (PK) study was designed as a proof-of-concept experiment to determine whether the optimized prodrugs could enhance systemic exposure of MBZ following oral administration. Applying a multi-parameter screening cascade evaluating pH-dependent solubility and stability, clearance, permeability, and bioactivation, with the latter both assessing intestinal versus hepatic compartments and cross-species human versus mouse differences, narrowed the series to three lead candidates for in vivo mouse PK evaluation. Prodrugs **2b**, **2c**, and **2i** were selected based on their different integrated in vitro profiles and were all evaluated against MBZ in mice. Prodrug **2i** demonstrated the most balanced in vitro profile, combining high intestinal solubility and permeability, minimal intestinal degradation across species, and hepatic bioactivation giving MBZ. Prodrug **2b**, which exhibited the highest intrinsic clearance among the selected candidates, was included as a comparator with a more dynamic in vitro profile.

The two major circulating metabolites of MBZ are the reduced metabolite **6a** and the metabolite **6b**, formed by hydrolysis of the carbamate [2,43], whereas metabolite **6c** has primarily been reported in urine [2,10] (Scheme 2). Intestinal metabolism of MBZ favors formation of the reduced metabolite **6a** via cytosolic enzymes, which are suggested to include carbonyl reductases, whereas both **6a** and **6b** are formed in the liver [25]. Since MBZ and its metabolites differ in exposure levels and elimination kinetics, the PK analysis monitored

systemic levels of parent MBZ, major MBZ metabolites and circulating intact prodrug. The total MBZ-related exposure was calculated as the sum of parent MBZ, metabolites **6a** and **6b**, and remaining prodrug where applicable, and was used as a proxy for total MBZ amount. Although metabolite **6c** was initially included in bioanalysis for **2b** and **2c**, its circulating levels following MBZ administration were negligible, and **6c** was therefore excluded from total exposure calculations across dose groups. This approach aligns with the clinical literature identifying **6a** and **6b** as the dominant circulating MBZ metabolites [2,10].



Scheme 2. The formation of the major metabolites of mebendazole (MBZ).

Oral administration of prodrugs **2b**, **2c**, and **2i** (at doses equimolar to 30 mg/kg MBZ) markedly increased systemic exposure of MBZ-related material compared to oral MBZ (Figure 4; Table 6). Notably, the primary pharmacokinetic enhancement was a pronounced ~3–10-fold increase in peak systemic concentration (C_{max}), whereas total systemic exposure ($AUC_{0\text{-}t}$) of MBZ-related material increased more modestly (~2-fold). In addition, the prodrugs demonstrated a substantially accelerated absorption profile, reaching peak parent MBZ concentrations much faster than when MBZ was dosed orally. In a follow-up study, prodrug **2i** was compared to MBZ at a lower equimolar dose, also confirming the results at lower doses (Figure S5; Table S2).

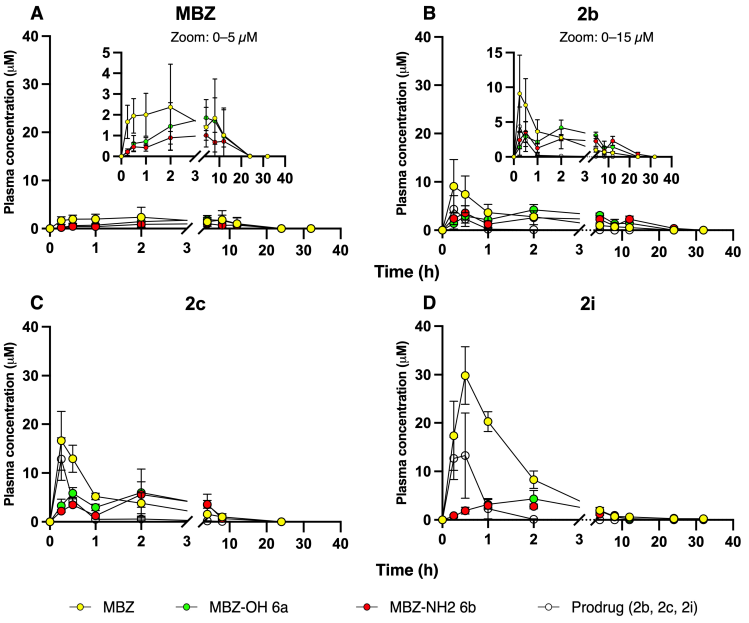


Figure 4. Concentration–time profiles of pharmacokinetic (PK) plasma samples of treatment groups with (**A**) mebendazole (MBZ), (**B**) prodrug **2b**, (**C**) prodrug **2c**, and (**D**) prodrug **2i**, with exposure curves for prodrugs, MBZ, and metabolites **6a** and **6b**. The test compounds were administered at an equimolar dose to MBZ. Prodrugs **2b** (55.2 mg/kg), **2c** (47.5 mg/kg) and **2i** (50.0 mg/kg), or MBZ (30 mg/kg) were orally administered to CD-1 mice. Nine mice were dosed in each group, and three samples were taken per animal. Data are presented as mean ± SD. MBZ is reported from two separate high-dose pharmacokinetic studies performed on different occasions. Insets in panels A and B show the same data on expanded concentration scales of 0–5 and 0–15 μM, respectively.

Table 6. In vivo PK results. Key pharmacokinetic parameters for parent MBZ after oral administration of MBZ (30 mg/kg) or prodrugs at equimolar doses.

Compound	C_{max} Prodrug (μM)	C_{max} MBZ (μM)	AUC * MBZ (μM × h)	AUC * MBZ Total ^ (μM × h)
MBZ	-	2.7 ± 1.4 #	26 ± 19 #	63 ± 35 #
2b	4.4 ± 2.8	9.1 ± 5.6	22 ± 2.8	98
2c	13 ± 4.4	17 ± 6.0	33 ± 4.1	96
2i	13 ± 8.8	30 ± 6.0	58 ± 3.4	110

* AUC represents AUC_{0-t} with t = last quantifiable time point of the experiment. For the prodrug groups, C_{max} values are reported as mean ± SD at the observed Tmax. MBZ AUC values were calculated from composite mean plasma concentration–time profiles and are reported as AUC ± SE obtained from GraphPad Prism. Because of the sparse-sampling design, these SE values do not represent standard deviations of individual-animal AUC values. ^ MBZ total includes MBZ-related material and is the sum of quantified MBZ, **6a**, **6b** and, where applicable, intact prodrug. # For the MBZ control, values are reported as mean ± SE calculated from the two separate high-dose PK studies (n = 2 study-level estimates), rather than from individual animals. C_{max}, maximum observed plasma concentration; MBZ, mebendazole; PK, pharmacokinetics.

An important limitation of the present pharmacokinetic comparison is that MBZ was administered as a suspension, whereas the prodrugs were administered as solutions. Differences in formulation and dissolution may therefore have contributed to the observed differences in C_{max} and time to maximum observed plasma concentration (T_{max}) (Figure 4, Table S2). Although the results demonstrate increased systemic MBZ exposure following the administration of selected prodrugs, the relative contributions of improved dissolution and prodrug-mediated absorption and bioactivation cannot be distinguished from these experiments alone. Further studies using formulation-matched comparators will be needed to clarify these contributions. The prodrugs were tested as the isolated regioisomeric mixtures as reported in the synthetic description in the supplementary material. The in vivo PK data generated could be influenced by the properties of the respective regioisomer and therefore also by the ratios of the isolated regioisomers. This was not considered at this stage, but will need to be addressed when progressed further. Nevertheless, despite these limitations, the increased systemic MBZ exposure observed following oral administration of the selected prodrugs provides proof-of-concept for the urea-based prodrug strategy and supports its further optimization.

The in vivo findings correlated well with the results obtained during in vitro profiling, as outlined in the screening cascade. Prodrug **2b**, which exhibited high clearance and rapid MBZ generation in vitro, yielded lower C_{max} and AUC_{0-t} values than **2c** and **2i** (Figure 4; Table 6). Overall, prodrug **2i** demonstrated the most favorable PK profile.

Taken together, these data provide in vivo proof-of-concept that urea-based prodrugs can successfully improve systemic exposure of MBZ after oral administration. Although it remains to be determined whether therapeutic efficacy is primarily driven by maximum peak exposure (C_{max}) or total systemic availability (AUC_{0-t}), these results demonstrate the utility of urea-based prodrugs for enhancing oral drug delivery.

3.4. Toxicity Assessment of Prodrugs, MBZ, Metabolites and Formed Promoieties

An important consideration for any prodrug strategy is that, in addition to the prodrugs, the released parent drug, metabolites and any additional promoieties formed are also well tolerated. For MBZ, the major circulating metabolites **6a** and **6b** have been described in clinical PK studies and often reach plasma exposures exceeding those of the parent compound, particularly during repeated dosing [43]. Although clinical experience with

MBZ has not identified these metabolites as major drivers of toxicity, this interpretation should be made cautiously given the generally low and variable systemic exposure achieved with conventional oral administration of MBZ.

To assess the potential cytotoxicity of the urea-based prodrug **2i**, MBZ-related metabolites, and prodrug-derived fragments, selected compounds were evaluated in HepG2 cells using a fluorometric microculture cytotoxicity assay (FMCA). This assay measures the fluorescence generated by the hydrolysis of fluorescein diacetate (FDA) to fluorescein by viable cells with intact plasma membranes. The tested compounds included MBZ, the major metabolites **6a** and **6b**, prodrug **2i**, and the cyclic urea fragment **3i** formed during the release of MBZ from prodrug **2i**. Compounds **6a**, **6b**, and **3i** showed no marked cytotoxic activity at the tested concentrations (Figures S3 and S4). Prodrug **2i** displayed intermediate cytotoxic activity, which was notably lower than that of MBZ itself.

These findings provide an initial assessment of cytotoxicity in HepG2 cells under the conditions tested. The major MBZ metabolites (**6a** and **6b**) and the released cyclic urea (**3i**) showed no marked cytotoxicity within the investigated concentration range. However, these results do not establish the systemic safety of the prodrugs or their metabolites and released fragments. Further studies, including repeated-dose toxicity assessments and formal toxicological evaluation, will be required before clinical development.

4. Conclusions

In this work, we demonstrate that a rational prodrug strategy exploring a chemically novel scaffold can successfully address the solubility and first-pass metabolic barriers limiting the systemic exposure of MBZ. Novel prodrugs, featuring a masked internal nucleophile as part of a self-immolative linker attached to a nitrogen atom in MBZ, were shown to be sufficiently soluble and stable under conditions mimicking gastrointestinal passage. Balancing permeability against comparative intestinal versus hepatic S9 metabolic clearance enabled us to prioritize candidates with profiles consistent with reduced intestinal metabolism and post-absorptive release of MBZ. Importantly, these prodrugs constitute a rare example in which an amino group in the parent molecule is the attachment point forming a urea prodrug, and this strategy could be further investigated.

The success of this platform relied on the seamless integration of medicinal chemistry, in vitro absorption, distribution, metabolism, and excretion (ADME) profiling, and in vivo pharmacokinetics, where synthetic efforts were guided by a compartmentalized ADME screening cascade. This multidisciplinary approach translated into in vivo pharmacokinetic proof-of-concept in mice. The most promising prodrug (**2i**), tested at two different doses, displayed improved systemic exposure of MBZ compared with oral equimolar MBZ. The proof-of-concept study holds clear potential for repositioning MBZ into systemic indications such as oncology and systemic lupus erythematosus (SLE). Moving forward, additional studies integrating dissolution-rate experiments, pharmacokinetic/pharmacodynamic (PK/PD) and physiologically based pharmacokinetic (PBPK) modeling, formulation development, and formal multi-dose toxicology studies that also consider the evaluation of the individual regioisomers will be essential before reaching the clinical setting.

Supplementary Materials: The following supporting information can be downloaded at https://www.mdpi.com/article/10.3390/pharmaceutics18111450/s1. The supporting information accompanying this article includes synthetic descriptions and analytical data (General experimental details, NMR studies of MBZ, General Synthetic Methodology, Figure S1, Synthesis of prodrug **2a-2k**, compounds **3i**, **4**, **5**, analytical documentation (^{1}H NMR spectra and LC-MS chromatograms) for the final compounds (for **3i** and **5** additional NMR spectra are included for structure elucidation), in vitro profiling (Table S1, Figure S2), toxicity assessments (Figures S3 and S4) and in vivo pharmacokinetics (High-

dose pharmacokinetic studies, Study conduct and deviations, Confirmatory low-dose pharmacokinetic study, Figure S5, Table S2). References [44–56] are cited in the supplementary materials.

Author Contributions: Conceptualization, K.F., Y.G., C.A., R.L., P.N. and M.F.; methodology, K.F., Y.G., R.S. and P.W.; investigation, K.F., Y.G., R.S., P.W., J.L. and C.B.; formal analysis, R.S., K.F., Y.G. and M.F.; data curation, R.S., K.F. and Y.G.; writing—original draft preparation, M.F., K.F., Y.G. and R.S.; writing—review and editing, all authors; supervision, K.F., Y.G., C.A., R.L., P.N. and M.F.; project administration, K.F., Y.G., C.A., R.L., P.N. and M.F.; funding acquisition, M.F., P.N. and R.L. All authors have read and agreed to the published version of the manuscript.

Funding: This research was funded by the Swedish Cancer Society (Cancerfonden, 22 1976 Pj-FD 1) and the Erling-Persson Foundation (Project ID 2022 0021). The article processing charge (APC) was funded by the Erling-Persson Foundation. The funders had no role in the design of the study; in the collection, analysis, or interpretation of data; in the writing of the manuscript; or in the decision to publish the results.

Institutional Review Board Statement: The animal studies were conducted in accordance with Swedish animal welfare regulations and were approved by Regional Animal Ethics Committee in Stockholm, Sweden (Stockholms djurförsöksetiska nämnd)in Stockholm, Sweden (approval nos. 4570-2019, approved 25 April 2019; 17114-2020, approved 28 January 2021; and 5082-25, approved 22 April 2025).

Informed Consent Statement: Not applicable.

Data Availability Statement: Additional data supporting the findings of this study are available in the Supplementary Materials or may be requested from the corresponding author.

Acknowledgments: The authors gratefully acknowledge the skillful technical contributions of Malin Berglund and Lena Lenhammar, the contributions of Per Arvidsson and Kristian Sandberg to the project, and the late Fredrik Klingegård for his contributions to the medicinal chemistry work.

Conflicts of Interest: Patents: The work described in this manuscript is related to international patent application PCT/EP2026/054258, published as WO 2026/175846 A1, entitled "Prodrugs of Benzimidazole Derivatives of Formula (I)".

Abbreviations

A→B, apical-to-basolateral transport; ADME, absorption, distribution, metabolism, and excretion; APC, article processing charge; ATCC, American Type Culture Collection; AUC, area under the plasma concentration–time curve; AUC_{0-t}, area under the plasma concentration–time curve from time zero to the last quantifiable time point; B→A, basolateral-to-apical transport; BCS, Biopharmaceutics Classification System; Bn, benzyl; CES1, carboxylesterase 1; CES2, carboxylesterase 2; CL_{int}, intrinsic clearance; $CL_{int,dep}$, intrinsic clearance of prodrug depletion; C_{max}, maximum observed plasma concentration; CV, coefficient of variation; CYP450, cytochrome P450; DCM, dichloromethane; DIPEA, diisopropylethylamine; DMF, N,N-dimethylformamide; DMSO, dimethyl sulfoxide; ER, efflux ratio; Et, ethyl; EtOAc, ethyl acetate; EtOH, ethanol; ESI, electrospray ionization; FaSSGF, fasted-state simulated gastric fluid; FaSSIF, fasted-state simulated intestinal fluid; FDA, fluorescein diacetate; FeSSIF, fed-state simulated intestinal fluid; FMCA, fluorometric microculture cytotoxicity assay; GI, gastrointestinal; HBSS, Hanks' balanced salt solution; HEPES, 4-(2-hydroxyethyl)-1-piperazineethanesulfonic acid; HI, human intestinal; HI-S9, human intestinal S9; HL, human liver; HL-S9, human liver S9; HPLC, high-performance liquid chromatography; IC_{50}, half-maximal inhibitory concentration; LC-MS/MS, liquid chromatography–tandem mass spectrometry; LLOQ, lower limit of quantification; MBZ, mebendazole; Me, methyl; MeOH, methanol; MI, mouse intestinal; MI-S9, mouse intestinal S9; ML, mouse liver; ML-S9, mouse liver S9; MRM, multiple reaction monitoring; MS, mass spectrometry; NADPH, reduced nicotinamide adenine dinucleotide phosphate; NMR, nuclear magnetic resonance; P_{app}, apparent permeability; PBPK, physiologically based pharmacokinetic; PBS, phosphate-buffered saline; PEG300, polyethylene glycol 300; Ph, phenyl;

PK, pharmacokinetics; PK/PD, pharmacokinetic/pharmacodynamic; S/N, signal-to-noise ratio; S9, supernatant fraction containing both cytosol and microsomes; SD, standard deviation; SI, survival index; SLE, systemic lupus erythematosus; t-Bu, tert-butyl; $T_{1/2}$, half-life; TDM, therapeutic drug monitoring; T_{max}, time to maximum observed plasma concentration; UPLC, ultra-performance liquid chromatography; UV, ultraviolet.

References

1. Edwards, G.; Breckenridge, A.M. Clinical Pharmacokinetics of Anthelmintic Drugs. *Clin. Pharmacokinet.* **1988**, *15*, 64–93. [CrossRef] [PubMed]
2. Dayan, A.D. Albendazole, Mebendazole and Praziquantel. Review of Non-Clinical Toxicity and Pharmacokinetics. *Acta Trop.* **2003**, *86*, 141–159. [CrossRef] [PubMed]
3. Guerini, A.E.; Triggiani, L.; Maddalo, M.; Bonù, M.L.; Frassine, F.; Baiguini, A.; Alghisi, A.; Tomasini, D.; Borghetti, P.; Pasinetti, N.; et al. Mebendazole as a Candidate for Drug Repurposing in Oncology: An Extensive Review of Current Literature. *Cancers* **2019**, *11*, 1284. [CrossRef] [PubMed]
4. Blum, C.B.; McMenamin, M.; Khoo, T.; Edwin, J.M.; Jose, P.; O'Callaghan, L.A. From Anthelmintic to Neuro-oncology: A Systematic Review of Mebendazole Repurposing for Brain Tumour Therapy. *Br. J. Clin. Pharmacol.* **2026**, bc70565. [CrossRef] [PubMed]
5. Rodrigues, D.C.D.N.; Porto, J.C.S.; Dos Santos, I.L.; Filho, J.I.A.B.; Ferreira, P.M.P. Repositioning Anthelmintics for the Treatment of Inflammatory-Based Pathological Conditions. *Inflammopharmacology* **2025**, *33*, 551–571. [CrossRef] [PubMed]
6. Bai, R.-Y.; Staedtke, V.; Rudin, C.M.; Bunz, F.; Riggins, G.J. Effective Treatment of Diverse Medulloblastoma Models with Mebendazole and Its Impact on Tumor Angiogenesis. *Neuro Oncol.* **2015**, *17*, 545–554. [CrossRef] [PubMed]
7. Eloranta, M.L.; Nygren, P.; Larsson, R.; Loskog, A.; Woodworth, N.; Hultqvist, M.; Svensson, R.; Gravenfors, Y.; Rönnblom, L.; Fryknäs, M. Efficacy of Mebendazole in the Spontaneous NZBxNZWF1 Animal Model of Systemic Lupus Erythematosus. *Sci. Rep.* **2026**, *16*, 6357. [CrossRef] [PubMed]
8. Mansoori, S.; Fryknäs, M.; Alvfors, C.; Loskog, A.; Larsson, R.; Nygren, P. A Phase 2a Clinical Study on the Safety and Efficacy of Individualized Dosed Mebendazole in Patients with Advanced Gastrointestinal Cancer. *Sci. Rep.* **2021**, *11*, 8981. [CrossRef] [PubMed]
9. Amidon, G.L.; Lennernäs, H.; Shah, V.P.; Crison, J.R. A Theoretical Basis for a Biopharmaceutic Drug Classification: The Correlation of in Vitro Drug Product Dissolution and in Vivo Bioavailability. *Pharm. Res.* **1995**, *12*, 413–420. [CrossRef] [PubMed]
10. Dawson, M.; Braithwaite, P.; Roberts, M.; Watson, T. The Pharmacokinetics and Bioavailability of a Tracer Dose of [3H]- Mebendazole in Man. *Br. J. Clin. Pharmacol.* **1985**, *19*, 79–86. [CrossRef] [PubMed]
11. Himmelreich, M.; Rawson, B.J.; Watson, T.R. Polymorphic Forms of Mebendazole. *Aust. J. Pharm. Sci.* **1977**, *6*, 123–125.
12. Swanepoel, E.; Liebenberg, W.; De Villiers, M.M. Quality Evaluation of Generic Drugs by Dissolution Test: Changing the USP Dissolution Medium to Distinguish between Active and Non-Active Mebendazole Polymorphs. *Eur. J. Pharm. Biopharm.* **2003**, *55*, 345–349. [CrossRef] [PubMed]
13. Bai, R.-Y.; Staedtke, V.; Wanjiku, T.; Rudek, M.A.; Joshi, A.; Gallia, G.L.; Riggins, G.J. Brain Penetration and Efficacy of Different Mebendazole Polymorphs in a Mouse Brain Tumor Model. *Clin. Cancer Res.* **2015**, *21*, 3462–3470. [CrossRef] [PubMed]
14. Brusau, E.V.; Camí, G.E.; Narda, G.E.; Cuffini, S.; Ayala, A.P.; Ellena, J. Synthesis and Characterization of a New Mebendazole Salt: Mebendazole Hydrochloride. *J. Pharm. Sci.* **2008**, *97*, 542–552. [CrossRef] [PubMed]
15. Camí, G.E.; Brusau, E.V.; Narda, G.E.; Maggio, R.M. Dual Approach for Concomitant Monitoring of Dissolution and Transformation at Solid-State. Mebendazole Salts Case Study. *J. Drug Deliv. Sci. Technol.* **2020**, *55*, 101344. [CrossRef]
16. Gutiérrez, E.L.; Godoy, A.A.; Brusau, E.V.; Vega, D.; Narda, G.E.; Suárez, S.; Di Salvo, F. Mebendazolium Mesylate Anhydride Salt: Rational Design Based on Supramolecular Assembly, Synthesis, and Solid-State Characterization. *RSC Adv.* **2024**, *14*, 181–192. [CrossRef] [PubMed]
17. García-Rodriguez, J.J.; De La Torre-Iglesias, P.M.; Vegas-Sánchez, M.C.; Torrado-Durán, S.; Bolás-Fernández, F.; Torrado-Santiago, S. Changed Crystallinity of Mebendazole Solid Dispersion: Improved Anthelmintic Activity. *Int. J. Pharm.* **2011**, *403*, 23–28. [CrossRef] [PubMed]
18. Singh, R.; Juneja, M.; Saini, V.; Malviya, R.; Kshirsagar, R.; Kashyap, M.; Sangamwar, A.T. Synergistic Approach of Salt Formation and Polymer-Mediated Stabilization to Enhance the Biopharmaceutical Performance of Mebendazole. *Eur. J. Pharm. Biopharm.* **2025**, *214*, 114809. [CrossRef] [PubMed]
19. Sumimoto, Y.; Okawa, S.; Inoue, T.; Masuda, K.; Maruyama, M.; Higaki, K. Extensive Improvement of Oral Bioavailability of Mebendazole, a Brick Dust, by Polymer-Containing SNEDDS Preparation: Disruption of High Crystallinity by Utilizing Its Counter Ion. *Eur. J. Pharm. Biopharm.* **2022**, *172*, 213–227. [CrossRef] [PubMed]

20. Ding, C.; Ding, Y.; Xu, Z.; Wang, P.; Xu, S. Preparation and Pharmacokinetic Study of Mebendazole Complex with HP-Beta-Cyclodextrin. *Front. Vet. Sci.* **2025**, *12*, 1611154. [CrossRef] [PubMed]
21. Dawson, M.; Watson, T.R. 4-Amino-3-(3′-Methoxycarbonyl-2′-Thioureido)Benzophenone, a Prodrug of Mebendazole. *Eur. J. Drug Metab. Pharmacokinet.* **1983**, *8*, 329–334. [CrossRef] [PubMed]
22. Nielsen, L.S.; Sløk, F.; Bundgaard, H. N-Alkoxycarbonyl Prodrugs of Mebendazole with Increased Water Solubility. *Int. J. Pharm.* **1994**, *102*, 231–239. [CrossRef]
23. Chassaing, C.; Berger, M.; Heckeroth, A.; Ilg, T.; Jaeger, M.; Kern, C.; Schmid, K.; Uphoff, M. Highly Water-Soluble Prodrugs of Anthelmintic Benzimidazole Carbamates: Synthesis, Pharmacodynamics, and Pharmacokinetics. *J. Med. Chem.* **2008**, *51*, 1111–1114. [CrossRef] [PubMed]
24. Zimmermann, S.C.; Tichý, T.; Vávra, J.; Dash, R.P.; Slusher, C.E.; Gadiano, A.J.; Wu, Y.; Jančařík, A.; Tenora, L.; Monincová, L.; et al. N-Substituted Prodrugs of Mebendazole Provide Improved Aqueous Solubility and Oral Bioavailability in Mice and Dogs. *J. Med. Chem.* **2018**, *61*, 3918–3929. [CrossRef] [PubMed]
25. Nishimuta, H.; Nakagawa, T.; Nomura, N.; Yabuki, M. Significance of Reductive Metabolism in Human Intestine and Quantitative Prediction of Intestinal First-Pass Metabolism by Cytosolic Reductive Enzymes. *Drug Metab. Dispos.* **2013**, *41*, 1104–1111. [CrossRef] [PubMed]
26. Zhao, J.; Zhang, B.; Mao, Q.; Ping, K.; Zhang, P.; Lin, F.; Liu, D.; Feng, Y.; Sun, M.; Zhang, Y.; et al. Discovery of a Colon-Targeted Azo Prodrug of Tofacitinib through the Establishment of Colon-Specific Delivery Systems Constructed by 5-ASA–PABA–MAC and 5-ASA–PABA–Diamine for the Treatment of Ulcerative Colitis. *J. Med. Chem.* **2022**, *65*, 4926–4948. [CrossRef] [PubMed]
27. Hubatsch, I.; Ragnarsson, E.G.E.; Artursson, P. Determination of Drug Permeability and Prediction of Drug Absorption in Caco-2 Monolayers. *Nat. Protoc.* **2007**, *2*, 2111–2119. [CrossRef] [PubMed]
28. Ghosh, A.K.; Brindisi, M. Organic Carbamates in Drug Design and Medicinal Chemistry. *J. Med. Chem.* **2015**, *58*, 2895–2940. [CrossRef] [PubMed]
29. Saari, W.S.; Schwering, J.E.; Lyle, P.A.; Smith, S.J.; Engelhardt, E.L. Cyclization-Activated Prodrugs. Basic Carbamates of 4-Hydroxyanisole. *J. Med. Chem.* **1990**, *33*, 97–101. [CrossRef] [PubMed]
30. Klein, S. The Use of Biorelevant Dissolution Media to Forecast the In Vivo Performance of a Drug. *AAPS J.* **2010**, *12*, 397–406. [CrossRef] [PubMed]
31. Abuhelwa, A.Y.; Williams, D.B.; Upton, R.N.; Foster, D.J.R. Food, Gastrointestinal pH, and Models of Oral Drug Absorption. *Eur. J. Pharm. Biopharm.* **2017**, *112*, 234–248. [CrossRef] [PubMed]
32. Teleki, A.; Nylander, O.; Bergström, C.A.S. Intrinsic Dissolution Rate Profiling of Poorly Water-Soluble Compounds in Biorelevant Dissolution Media. *Pharmaceutics* **2020**, *12*, 493. [CrossRef] [PubMed]
33. Kambayashi, A.; Shirasaka, Y. Food Effects on Gastrointestinal Physiology and Drug Absorption. *Drug Metab. Pharmacokinet.* **2023**, *48*, 100488. [CrossRef] [PubMed]
34. Rodriguez-Caabeiro, F.; Criado-Fornelio, A.; Jimenez-Gonzalez, A.; Guzman, L.; Igual, A.; Perez, A.; Pujol, M. Experimental Chemotherapy and Toxicity in Mice of Three Mebendazole Polymorphic Forms. *Chemotherapy* **1987**, *33*, 266–271. [CrossRef] [PubMed]
35. Charoenlarp, P.; Waikagul, J.; Muennoo, C.; Srinophakun, S.; Kitayaporn, D. Efficacy of Single-Dose Mebendazole, Polymorphic Forms A and C, in the Treatment of Hookworm and Trichuris Infections. *Southeast Asian J. Trop. Med. Public Health* **1993**, *24*, 712–716. [PubMed]
36. Dahan, A.; Miller, J.M. The Solubility–Permeability Interplay and Its Implications in Formulation Design and Development for Poorly Soluble Drugs. *AAPS J.* **2012**, *14*, 244–251. [CrossRef] [PubMed]
37. O'Shea, J.P.; Augustijns, P.; Brandl, M.; Brayden, D.J.; Brouwers, J.; Griffin, B.T.; Holm, R.; Jacobsen, A.-C.; Lennernäs, H.; Vinarov, Z.; et al. Best Practices in Current Models Mimicking Drug Permeability in the Gastrointestinal Tract-An UNGAP Review. *Eur. J. Pharm. Sci.* **2022**, *170*, 106098. [CrossRef] [PubMed]
38. Artursson, P.; Karlsson, J. Correlation between Oral Drug Absorption in Humans and Apparent Drug Permeability Coefficients in Human Intestinal Epithelial (Caco-2) Cells. *Biochem. Biophys. Res. Commun.* **1991**, *175*, 880–885. [CrossRef] [PubMed]
39. Kus, M.; Ibragimow, I.; Piotrowska-Kempisty, H. Caco-2 Cell Line Standardization with Pharmaceutical Requirements and In Vitro Model Suitability for Permeability Assays. *Pharmaceutics* **2023**, *15*, 2523. [CrossRef] [PubMed]
40. Carlert, S.; Åkesson, P.; Jerndal, G.; Lindfors, L.; Lennernäs, H.; Abrahamsson, B. *In Vivo* Dog Intestinal Precipitation of Mebendazole: A Basic BCS Class II Drug. *Mol. Pharm.* **2012**, *9*, 2903–2911. [CrossRef] [PubMed]
41. Lentz, K.A.; Polli, J.W.; Wring, S.A.; Humphreys, J.E.; Polli, J.E. Influence of Passive Permeability on Apparent P-Glycoprotein Kinetics. *Pharm. Res.* **2000**, *17*, 1456–1460. [CrossRef] [PubMed]
42. Varma, M.V.S.; Sateesh, K.; Panchagnula, R. Functional Role of P-Glycoprotein in Limiting Intestinal Absorption of Drugs: Contribution of Passive Permeability to P-Glycoprotein Mediated Efflux Transport. *Mol. Pharm.* **2005**, *2*, 12–21. [CrossRef] [PubMed]

43. Braithwaite, P.A.; Roberts, M.S.; Allan, R.J.; Watson, T.R. Clinical Pharmacokinetics of High Dose Mebendazole in Patients Treated for Cystic Hydatid Disease. *Eur. J. Clin. Pharmacol.* **1982**, *22*, 161–169. [CrossRef] [PubMed]
44. Ke, F.; Zhang, P.; Lin, C.; Lin, X.; Xu, J.; Zhou, X. Synthesis of benzimidazoles by CuI-catalyzed three-component reaction of 2-haloaniline, ammonia and aldehyde in water. *Org. Biomol. Chem.* **2018**, *16*, 8090–8094. [CrossRef] [PubMed]
45. Nelli, M.R.; Cantrell, R.L.; Looper, R.E. Gold Catalyzed 7-*endo*-dig Hydroaminations Yielding 1,4-Diazepineones. *J. Org. Chem.* **2023**, *88*, 15975–15982. [CrossRef] [PubMed]
46. Chapman, R.G.; Ostuni, E.; Takayama, S.; Holmlin, R.E.; Yan, L.; Whitesides, G.M. Surveying for Surfaces that Resist the Adsorption of Proteins. *J. Am. Chem. Soc.* **2000**, *122*, 8303–8304. [CrossRef]
47. Corso, A.D.; Borlandelli, V.; Corno, C.; Perego, P.; Belvisi, L.; Pignataro, L.; Gennari, C. Fast Cyclization of a Proline-Derived Self-Immolative Spacer Improves the Efficacy of Carbamate Prodrugs. *Angew. Chem. Int. Ed.* **2019**, *59*, 4176–4181. [CrossRef] [PubMed]
48. Xu, Z.; Wheeler, K.A.; Baures, P.W. Parallel Synthesis of Peptide-Like Macrocycles Containing Imidazole-4,5-dicarboxylic Acid. *Molecules* **2012**, *17*, 5346–5362. [CrossRef] [PubMed]
49. de Groot, F.M.H.; Loos, W.J.; Koekkoek, R.; van Berkom, L.W.A.; Busscher, G.F.; Seelen, A.E.; Albrecht, C.; de Bruijn, P.; Scheeren, H.W. Elongated Multiple Electronic Cascade and Cyclization Spacer Systems in Activatible Anticancer Prodrugs for Enhanced Drug Release. *J. Org. Chem.* **2001**, *66*, 8815–8830. [CrossRef] [PubMed]
50. Liu, B.; Yu, T.; Zhang, Y.; Zhang, X.; Zhang, S.; Cheng, C.; Zhang, J. Heteroaromatic Derivatives and Pharmaceutical Applica-tions Thereof. WO2015161830A1, 29 October 2015.
51. Poeschinger, T.; Ries, C.; Shen, H.; Yun, H.; Hoves, S.; Hage, C. 7-Substituted Sulfonimidoylpurinone Compounds and Deriva-tives for the Treatment and Prophylaxis of Liver Cancer. US20200268762A1, 27 August 2020.
52. Thomsen, K.F.; Strøm, F.; Sforzini, B.V.; Begtrup, M.; Mørk, N. Evaluation of phenyl carbamates of ethyl diamines as cyclization-activated prodrug forms for protecting phenols against first-bass metabolism. *Int. J. Pharm.* **1994**, *112*, 143–152. [CrossRef]
53. Jacobson, I.C.; Lee, S.S.; Pizarro Novoa, J.C. Peptidomimetic N5-Methyl-N2-(Nonanoyl-L-Leucyl)-L-Glutaminate Derivatives, Triazaspiro[4.14]Nonadecane Derivatives and Similar Compounds as Inhibitors of Norovirus and Coronavirus Replication. WO2021188620, 23 September 2021.
54. Nelissen, J.; Lemkens, P.; Sann, H.; Bindl, M.; Bassissi, F.; Jasserand, D.; De Mey, J.; Janssen, B. Pharmacokinetic and pharmacodynamic properties of SOL1: A novel dual inhibitor of neutral endopeptidase and endothelin converting enzyme. *Life Sci.* **2012**, *91*, 587–592. [CrossRef] [PubMed]
55. Ronald, K.; Scott, D.K.; Nigel, L.; Gang, Z. Ethyldiamine Orexin Receptor Antagonists. WO2016100161A1, 23 June 2016.
56. Remers, W.A.; Iyengar, B.S.; Dorr, R.T.; Wisner, L.; Bates, R.B. Synthesis and Antitumor Activity of Heterocycles Related to Carbendazim. *J. Heterocycl. Chem.* **2014**, *52*, 136–141. [CrossRef]

Disclaimer/Publisher's Note: The statements, opinions and data contained in all publications are solely those of the individual author(s) and contributor(s) and not of MDPI and/or the editor(s). MDPI and/or the editor(s) disclaim responsibility for any injury to people or property resulting from any ideas, methods, instructions or products referred to in the content.